Angewandte
Eine Zeitschrift der Gesellschaft Deutscher Chemiker
Chemie

Supporting Information

Monodisperse Cylindrical Micelles of Controlled Length with a Liquid-Crystalline Perfluorinated Core by 1D "Self-Seeding"

Xiaoyu Li, Bixin Jin, Yang Gao, Dominic W. Hayward, Mitchell A. Winnik, Yunjun Luo,* and Ian Manners**

anie_201604551_sm_miscellaneous_information.pdf

Materials and Equipment.

All chemicals were purchased from Aldrich and were used as received unless otherwise stated. Diphenylethylene, dimethylsilacyclobutane, 2-vinyl pyridine (2VP), 2-(perfluorooctyl)ethyl methacrylate (FMA) and 2-mercaptoethanol were distilled over CaH_2 before use. For the anionic polymerizations, THF was pre-dried with Na before being distilled over Na/benzophenone under nitrogen. All of the self-assembly experiments were performed in HPLC grade solvents that were acquired from Fisher. 1H,1H-perfluorooctylamine was purchased from Santa Cruz Biotechnology. BODIPY® FL NHS ester was purchased from ThermoFisher Scientific.

NMR spectra were recorded at ambient temperatures on a Varian 400 spectrometer with reference to residual NMR solvent resonances.

Molecular weights and polydispersity indexes (M_w/M_n) of polymers were obtained by Gel Permeation Chromatography (GPC) using a Viscotex GPCmax Chromatograph equipped with automatic sampler, pump, injector, inline degasser, column oven (30 ^oC), styrene/divinylbenzene columns with pore sizes of 500 Å and 100 000 Å, VE 3580 refractometer, and the UV-vis signal was monitored at 440 nm. Butylated hydroxytoluene (0.025%, w.t.) stabilized THF (Fisher) containing 0.9 g/L $[Bu_4N]Br$ (to minimize interactions between basic sites on the polymer and the column) was used as the eluent, with a flow rate of 1.0 mL / min. Samples were dissolved in the eluent (2 mg / mL) and filtered (Acrodisc, PTFE membrane, 0.45 mm) before analysis. The calibration of refractive index detector was carried out using polystyrene standards (Viscotek).

Dynamic light scattering (173°) experiments were performed using a nano series Malvern zetasizer instrument equipped with a 633 nm red laser. Samples were analyzed in 1 cm glass cuvettes at 25 ^oC. For the purpose of the light scattering studies the refractive index of the block copolymers involved was assumed to be 1.60. The results of dynamic light scattering studies are reported as apparent hydrodynamic radius ($R_{h,\ app}$), acknowledging that the particles have been modelled as hard spheres in the experiments conducted.

For wide-angle X-ray scattering (WAXS) measurement of the polymer sample, polymer solution (~5 mg / mL in THF) was drop cast onto a glass slide to form a thin film. The sample was then vacuum-dried at room temperature for 24 h. WAXS analysis was performed at 25 ^oC using a X' Pert Pro MPD (PANalytical, Netherland) diffractometer operated at 40 kV and 40 mA with Cu Kα radiation (λ = 0.154 06 nm) . The data were collected at a scan rate of 0.01° s^{-1}.

Small-, medium- and wide-angle X-ray scattering (SAXS, MAXS and WAXS) measurements of the dried cylindrical micelles were performed in transmission geometry using a Ganesha small angle X-ray scattering apparatus (SAXSLAB, Denmark). The instrument uses copper Kα radiation (1.5 Å) and the scattering pattern is detected on a moveable 2-dimensional Pilatus 300K X-Ray Detector (Dectris, Switzerland). The concentrated cylindrical micelle solution was drop cast onto a 25 μm thick film of poly(4,4'-oxydiphenylene-pyromellitimide) (Kapton® HN, DuPont), a material often used in X-ray applications due to its high transmittance and mechanical strength, and the sample was secured in position, perpendicular to the

X-ray beam. The detector was positioned at a distance of approximately 1050 mm, 450 mm and 100 mm for the SAXS, MAXS and WAXS measurements respectively and the instrument was evacuated during measurement to reduce air scattering. As the instrument has been calibrated to give absolute intensities for each configuration, the data sets could be separately background subtracted and azimuthaly regrouped and subsequently overlaid and stitched together without introducing any further scaling factors.

Scanning Calorimetry (DSC) and thermogravimetric analysis (TGA) analyses were performed on the Q100 & Q500 from TA instruments at heating/cooling rates of 10 ^{o}C min^{-1}. The DSC was coupled to a refrigerated cooling system (RCS90).

UV-vis data were acquired from a Lambda 35 spectrometer using standard quartz cells from wavelength of 300 nm to 700 nm. Fluorescence data were obtained from a Perkin Elmer LS 45 Fluorescence Spectrometer.

Transmission Electron Microscopy (TEM)

The samples for electron microscopy were prepared by drop-casting one drop (ca. 10 μL) of the micelle colloidal solution onto a carbon coated copper grid which was placed on a piece of filter paper to remove excess solvent. Bright field TEM micrographs were obtained on a JEOL1200EX II microscope operating at 120 kV and equipped with an SIS MegaViewIII digital camera. No staining was applied for TEM samples unless stated otherwise. Images were analyzed using the ImageJ software package developed at the US National Institute of Health. For the statistical length analysis, over 200 cylinders were carefully traced manually to determine the contour length.

Micelle length distributions were determined using the software program ImageJ from the U.S. National Institutes of Health. For each sample, ca. 100 micelles in several images were traced by hand in order to obtain the length information. The number average micelle length (L_n) and weight average micelle length (L_w) were calculated using eq. S1 from measurements of the contour lengths (L_i) of individual micelles, where N_i is the number of micelles of length L_i, and n is the number of micelles examined in each sample.

$$L_n = \frac{\sum_{i=1}^{n} N_i L_i}{\sum_{i=1}^{n} N_i} \quad \text{(S1)}$$

$$L_w = \frac{\sum_{i=1}^{n} N_i L_i^2}{\sum_{i=1}^{n} N_i L_i} \quad \text{(S2)}$$

The distribution of micelle lengths is characterized by both L_w / L_n and the standard deviation of the length distribution σ.

Synthesis of P2VP$_{68}$-*b*-PFMA$_{41}$.

The diblock copolymer P2VP$_{68}$-*b*-PFMA$_{41}$ used in this study was synthesized via anionic polymerization in an inert atmosphere glovebox. All the molecular characteristics of the diblock copolymer are listed in Table S1 and the ^{1}H NMR spectrum is shown in Figure S2.

The detailed polymerization procedures are described as following: 2-vinyl

pyridine (500 mg, 4.7mmol) was dissolved in 15.0 mL THF at -78 ^{o}C, into which 42 mg of LiCl was added. Into the solution, a premixed solution of 1, 1-diphenylethylene (0.23 mmol, 41 μL) and *n*-butyl lithium (1.6 M in hexanes, 49 μL, 0.078 mmol) was added. The solution was allowed to stir at -78 ^{o}C for 1 h before 0.5 mL of aliquot was taken out and quenched to characterize the P2VP homopolymer. The solution was kept at -78 ^{o}C, and subsequently 1, 1-diphenylethylene (41 μL, 0.23 mmol) was added and the solution was allowed to stir for another 30 min. Then a precooled mixture of FMA (1.2 g. 0.0754 mmol), LiCl (20 mg) in 10 mL of THF was added into the solution. After stirring for another 1 h, 2 mg of 4-*tert*-butylphenol was added into the solution to quench the anion. The polymer was precipitated into hexane and was isolated as a white solid (yield = 76 %).

Preparation of seed cylindrical micelles.

Seed cylinders were prepared by ultrasonicating the block copolymer cylinders at low temperature. The original, polydisperse cylinders were obtained by directly dispersing the diblock copolymers into *i*-PrOH, and the solution was heated at 80 ^{o}C for 1 h before the solution was allowed to cool down naturally to room temperature. Then, the cylinders were sonicated (50W sonication processor equipped with a titanium sonotrode) at 0 ^{o}C for 4 h.

Self-seeding of seed cylindrical micelles.

The self-seeding of seed cylindrical micelles was performed by thermal annealing the seed samples at the desired concentration in a preset oil bath for 1 h (unless mentioned elsewhere). The oil bath was then turned off and the sample was allowed to cool down gradually to room temperature (23 ^{o}C) over a period of several hours, which is dependent on the annealing temperatures, ranging from 1 h (35 ^{o}C) to 6h (80 ^{o}C).

Synthesis of the F-dye molecule.

The schematic synthesis route for the F-dye molecule is shown in Figure S14(c). Typically, 5 mg of green dye (BODIPY-FL, 0.013 mmol of succinimidyl ester groups) was mixed with 100 mg of 1H,1H-perfluorooctylamine (0.22 mmol of amino groups), 1 mg of dicyclohexylcarbodiimide (8×10^{-3} mmol) and 0.8 mg of 4-dimethylaminopyridine (1×10^{-3} mmol) in dry THF (2 mL). The solution was stirred at room temperature for 3 days. The product mixture was purified using a silica gel column with *n*-butyl acetate : hexane = 1 : 1 (volume) as the eluent. A red solid was obtained by removing the solvent under vacumm and yield was 80 %. A ^{1}H NMR spectrum of the F-dye molecule is included in Figure S15.

Preparation of F-dye-loaded cylindrical micelles via F-TA process.

To prepare the cylindrical micelles with loading ratio of 3 % by mass, 0.2 mg of F-dye was added to the seed solution (0.1 mg / mL, 2 mL) (for loading ratio of 11 % by mass, 1 mg of F-dye was used). The solution was then thermally annealed at 80 ^{o}C for 1 h and then cooled to room temperature (23 ^{o}C). The excess of the dye molecules was removed by dialysis (cutoff 12000~14000 Dal) in the dark against *i*-PrOH for 5

days (the solvent was changed three times per day).

To calculate the amount of F-dye loaded in the cylindrical micelles, the UV-vis absorbance intensity was combined with the extinction coefficient of the BODIPY-FL dye molecules, via Lambert-Beer law. Thus, two assumptions were made for the calculation. Firstly, the amount of free F-dye is negligible after the dialysis. Secondly, the extinction coefficient of the F-dye remains the same as that of BODIPY-FL (80,000 M^{-1} cm^{-1}).

Additional discussion about the liquid crystalline nature of PFMA block.

From DSC traces, the diblock copolymer showed a phase transition at 84 °C with an enthalpy of 2.8 J /g of PFMA (Figure S3(b)). Both the temperature and enthalpy are comparable with the literature values for a smectic (either Sm A or Sm B) to isotropic phase transition in similar diblock copolymers containing fluorinated liquid crystalline side chains.[1] WAXS from the diblock at room temperature, shows a strong, broad peak centered at scattering vector of 12.4 nm^{-1} (Figure S3(c)). This corresponds to a periodicity of 0.52 nm, the expected average spacing between two mesogenic groups in a smectic phase.[1,2] By fitting the peak to a Pearson type VII distribution, it was possible to characterize the peak as approximately Lorentzian (with an exponent of 1.6) with a correlation length of 3.2 nm. The short correlation length and liquid-like side chain ordering suggested by the Lorentzian peak both favor the characterization of the phase as a smectic A as opposed to smectic crystal B (where one would expect a very sharp peak).[3,4]

Results from the small-, medium-, and wide-angle X-ray scattering from drop cast micelle films are shown in Figure 1(b). It is possible to assign the observed peaks to three characteristic length scales: peaks at q = 0.36 and q = 0.72 nm^{-1} correspond to the first and second order peaks associated with a periodicity of 17.4 nm, this is assigned to the diameter of the cylindrical micelles. At first glance, these peaks may appear similar to strong form factor peaks from the radius of the cylinders. However, these would not appear in the ratio 1:2 as is seen in the data. Secondly, the shape of these peaks does not correspond to the rounded Bessel function type one would expect from the form factor of monodisperse cylinders. In fact, fits reveal them to be approximately Lorentzian in character. Assuming the micelles are not close packed but are in discrete layers in the dried drop (where the layer thickness is equal to the diameter), this agrees well with TEM observations. (As measured from the TEM images, the diameter of the cylindrical micelles was 18.1 ± 1.2 nm). It should be noted that concentrated solutions of rods would be expected to pack into hexagonal structures. However, due to the manner in which these samples were prepared, repeated drop-casting onto a substrate followed by rapid evaporation of the solvent, it is unlikely that the micelles will have had time to form a well-ordered phase before drying. The result of this is a large fractal aggregate structure (which manifests in our data as the power-law behavior with an exponent of -3.3 in the low-Q region). Previous work has also shown that removing solvent from hexagonally-packed cylindrical micelles destroys the hexagonal ordering.[8] We postulate that the drop-by-drop addition onto a substrate and subsequent rapid removal of solvent results in disordered layers of micelles stacked with a spacing roughly equivalent to

their diameter. Unfortunately it is not easy to prove this via SEM as the structures are non-conductive and would require coating prior to imaging, we would therefore not have the sub 20 nm resolution required to observe the micelles in this way.

The sharp peaks observed at q = 2.02 nm^{-1} and q = 4.04 nm^{-1} correspond to a long-range periodicity of 3.3 nm, the average spacing between smectic layers in PFMA.[1,2] Finally, the peak at 12.4 nm^{-1} corresponds to a side-group spacing of 0.51 nm, in line with the value from the bulk sample. A schematic illustration of the LC core of the cylindrical micelles is included in Scheme S1. As before, the peak was fitted to a Pearson type VII distribution, revealing a correlation length of 2.7 nm. As the correlation length is much smaller than the dimensions of the micelle, this cannot be attributed to particle size-broadening effects (in contrast to crystalline-coil PFS-based micelles where the amount of broadening corresponds almost exactly to the diameter of the micelle[5]) indicating that the core of the micelles is indeed liquid crystalline.

Whilst a correlation length of five molecular widths (2.7 / 0.51 = 5.3) is typical of smectic A,[3,6] it was observed that the shape of the peak at 12.4 nm^{-1} appears to be square-root Lorentzian (with an exponent of 0.50), often considered to be a characteristic of hexatic ordering with quasi-long-range hexagonal orientational ordering but only short-range translational ordering as may be found in a hexatic smectic B for example.[7] It is therefore not possible to definitively assign the micelle core to either phase without further detailed measurements.

Additional discussion on "self-seeding" process.

The data in Figure 2(d) suggest that the length of the micelles should increase exponentially with the increase in annealing temperature. To test this idea, we replotted the data of Figure 2(c) in Figure S7 as $ln(L_n)$ versus 1000/T. In the range of 35 to 75 ^oC, the data fit well to this Arrhenius-type plot. Setting the slope of the plot equal to -E/RT, where R is the gas constant, we calculate an E value of 69 kJ mol^{-1}. Since micelle elongation operates under thermodynamic rather than kinetic control, this E value must be related to thermodynamic factors, for example, the enthalpy of dissolution of the micelles in *i*-PrOH. It is noteworthy that this value is much smaller than that reported for PFS systems (149 kJ mol^{-1}).[5]

From DSC traces (Figure S3(b)), the LC phase transition of PFMA is 2.8 J /g of PFMA, comparable to the results reported by Liu.[1] The smectic-to-isotropic phase transition enthalpy is much smaller than the crystallization energy from other crystalline block copolymers reported for CDSA. They are, however, much smaller than the melting enthalpies of crystalline polymers. Linear polyethylene, for example, exhibits decreasing melting enthalpies, ranging between 30 and 69 J / g, as its molecular weight is decreased.[11] For another example, this value is reported to range between 7.7 and 14.7 J / g for PFS systems.[12] This lower phase-transition energy is consistent with our finding mentioned above that the enthalpy of dissolution of these micelles (69 kJ mol^{-1}) in our study is smaller than that in PFS systems (149 kJ mol^{-1}).[9]

As can be observed from the TEM images of the cylindrical micelles produced via self-seeding (Fig. 2), the central sections, which correspond to the original seeds, are clearly thicker than the terminal segments. There are several possible reasons for this.

For example, the thicker section may be due to a higher degree of ordering of the LC phase in the core of the seed. In the original long cylindrical micelles, the degree of ordering may not be uniform along the whole cylindrical micelles, and only those with a higher degree of ordering survive the ultrasonication and heating (self-seeding) step.

Additional discussion on the plots in Figure 2(c) and 2(d).

In Figure 2(c) in the main text, we present a plot showing the average contour length vs. annealing temperature. This data illustrates that the length of the micelles increases with the annealing temperature, giving fibers up to values of ca. 800 nm with a narrow length distribution (L_w / L_n < 1.1).

Since the mass of polymer m in solution is constant, the length of micelles L_n is related to the total number of micelles N by equation (S3), if we assume i) the concentration of free polymer chains at 23 °C is negligible, ii) the mass of polymer per unit length M_L remains constant.

$$L_n = \frac{m}{M_L N} \quad \text{(S3)}$$

However for the first assumption, we could not rule out the possibility of the presence of unimers in the micelle solution. Nevertheless, we checked the micelle solutions that were subjected to the annealing treatment six months after the sample preparation and found the length of the cylindrical micelles did not show obvious increase (Table S7, Figure S13). For example, 16 h after sample preparation (0.1 mg / mL), micelles formed after the fragment solution was annealed at 70 °C were characterized by L_n = 462 nm and L_w / L_n = 1.03, these values changed to L_n = 460 nm and L_w / L_n = 1.04 six months after sample preparation. These results suggest that any unimers in solution at 23 °C do not have a significant effect on the length of micelles. The concentration of unimers is expected to be very low due to incompatibility between PFMA block and the hydrophilic solvent.

Based on Equation S3, we could calculate the fraction of seeds that survived the annealing at each temperature by taking into account the initial length of the fragments and the final length after annealing. The results are summarized in Figure 2(d).

Additional comment on the attempts to use seeded-growth to prepare uniform cylindrical micelles.

Several block copolymers with crystalline core-forming blocks have been reported to undergo seeded-growth process.[13-16] Since the micelles of $P2VP_{68}$-*b*-$PFMA_{41}$ can undergo self-seeding, it is reasonable to expect that they can undergo seeded-growth as well. Our first attempt was to directly add dissolved polymer solution (chloroform, 2.0 mg / mL) into the *i*-PrOH dispersion of seeds (1.0 mL, 0.01 mg / mL, L_n = 42 nm, PDI = 1.07). However, after being aged at 23 °C for more than a month (Figure S12(a)), we could only observe a large amount of short cylindrical micelles or spherical micelles (roughly 50-60 nm in length or diameter). The dissolved polymer formed small aggregates, which could hardly be distinguished from the seeds. We also used α, α, α-trifluorotoluene, trifluoroethanol and 2,2,3,3,3-pentafluoro-1-propanol as

the solvent for the unimer and tried the seeded growth experiment, but similar results were obtained.

Our previous study demonstrated that self-seeded micelles can facilitate the seeded-growth process.[13] Therefore, we used cylindrical micelles, which were thermally annealed at 50 °C for 60 min and then cooled to 23 °C, as the seed micelles to initiate the growth. The cylindrical micelles were aged at 23 °C for 24 h before being used for seeded-growth (L_n = 146 nm, PDI = 1.07).

We added chloroform solution (10 μL) of $P2VP_{68}$-*b*-$PFMA_{41}$ (2.0 mg / mL) into the *i*-PrOH dispersion of preannealed cylindrical micelles (1.0 mL, 0.01 mg / mL, preannealed at 50 °C, L_n = 146 nm, PDI = 1.07). The addition was conducted at 23 °C and the sample was characterized by TEM after stored at 23 °C for 24 h. However, instead of observing longer cylindrical micelles, we could only observe the mixture of original cylindrical seed micelles (L_n = 140 nm) and very short micelles (L_n = 72 nm and PDI = 1.21), as shown in Figure S12(b).

We also added the chloroform solution to the *i*-PrOH solution of cylindrical micelles at an elevated temperature (45 °C), and kept all other conditions exactly the same as in the previously described experiment. The L_n of cylindrical micelles increased from 146 nm to 207 nm (PDI = 1.12), and also large amount of very short micelles (L_n = 63 nm and PDI = 1.11) were observed (Figure S12(c)).

A plausible reason for the unsuccessful seeded growth is that due to the high fluorine content of the PFMA block, the compatibility between the core-forming block and the hydrophilic hydrocarbon solvent (*i*-PrOH) is extremely low. Thus when the molecularly dissolved $P2VP_{68}$-*b*-$PFMA_{41}$ diblock copolymer (in the form of unimers) is added into the *i*-PrOH dispersion of cylindrical micelles, the unimers tend to aggregate quickly and undergo self-nucleation. This leads to the formation of very short micelles rather than seeded growth from the existing seeds.

Additional analysis of the end-coupled cylindrical micellces.

When the cylindrical micelles at 0.1 mg / mL were aged at 23 °C for 6 months, no noticeable amount of cylindrical micelles underwent end-to-end coupling (Figure S13(a)). However, when the micelle concentration was increased to 0.2 mg / mL, though the population of end-coupled cylindrical micelles was very small (less than 1 %, Figure S13 (b)) in the freshly annealed sample, this value increased to 13 % after 6 month of storage at 23 °C (Figure S13(c)).

Among the cylindrical micelles at 0.2 mg / mL and aged at 23 °C for 6 months (Figure S13(c)), by TEM 75 % of the original cylindrical micelles still remained uncoupled after 6 months of storage, and 25 % of them underwent end-to-end coupling. To amplify, by counting over 400 nanoobjects from 10 TEM images, 13% of all the nanoobjects were end-coupled cylindrical micelles. Among these end-coupled micelles, 74 % are consisted of two original micelles, 24 % of three, and 2 % of four or more. The L_w, L_n and L_w / Ln were changed to 618 nm, 519 nm and 1.19, respectively.

As mentioned in the main text, the percentage population of end-coupled cylindrical micelles increased with the solution concentration and aging time. Thus, it is reasonable to speculate that end-to-end coupling observed in the current study is

most likely a probability issue. The end-coupling requires two cylindrical micelles to collide with the correct orientation in the solution state. The probability of such an event can be increased by using either a higher concentration or a longer storage period. A more systematic study is underway to explore this.

As mentioned in the manuscript, several factors (such as attachment of cylindrical micelles and matching of their crystalline planes, presence of homopolymer of the core-forming block, or covalent connection of the cylinders) can lead to the end-to-end coupling of cylindrical micelles. In our case, the most likely explanation will be similar to the first one, and the others can be ruled out. Firstly, the diblock copolymer $P2VP_{68}$-*b*-$PFMA_{41}$ was synthesized via sequential anionic polymerization, and thus only P2VP homopolymer but not PFMA homopolymer, would be expected as a trace impurity during the polymerization. Secondly, even if a trace amount of P2VP homopolymer is present in the solution, it is not likely that it causes the end-to-end coupling, since it is completely soluble in *i*-PrOH and not interactive with the cylindrical micelles.

As pointed out by Xu and coworkers,[16] the growth by end-coupling of short semicrystalline cylindrical micelles can take place only when the ends of two short cylindrical semicrystalline micelles collide, and the growth cannot proceed due to the mismatch of the crystal planes when the side part of a cylindrical micelle collides with the end of another cylindrical micelle. Similarly in our case, we didn't observe any end-to-side coupling, but only end-to-end coupling. This suggests that although the PFMA core is LC, it still requires the LC phase to orient approximately in the same direction for the end-to-end coupling. Another very obvious reason for the lack of end-to-side coupling is the steric stabilization effect provided by the corona chains.

Table S1 Molecular characteristics of $P2VP_{68}$-*b*-$PFMA_{41}$

M_n[a]	M_w[a]	M_w/M_n[a]	M_n of P2VP[b]	m/n[c]	m	n[d]
26 kDa	29 kDa	1.12	7.2 kDa	1.66	68	41

[a]: obtained from GPC; [b]: obtained from MALDI-TOF; [c]: obtained from ^{1}H NMR integration; [d]: calculated by combining the results from MALDI-TOF and ^{1}H NMR. m and n are the degree of polymerization of P2VP and PFMA block, respectively.

Table S2 Values of L_n, L_w, L_w/L_n, σ and σ/L_n of $P2VP_{68}$-*b*-$PFMA_{41}$ micelles formed after the seed solution was annealed at different temperatures for 1 h followed by cooling to 23 ^oC. Representative TEM images are included in Figure S6.

T (^oC)	L_n (nm)	L_w (nm)	L_w/L_n	σ (nm)	σ/L_n
35	51	54	1.06	13	0.25
40	73	77	1.05	17	0.23
45	105	111	1.06	26	0.25
50	146	156	1.07	38	0.26
55	193	201	1.04	38	0.20
60	241	251	1.04	49	0.20
65	324	334	1.03	52	0.16
70	462	471	1.02	65	0.14
75	801	817	1.02	123	0.15

Table S3 Values of L_n, L_w, L_w/L_n, σ and σ/L_n of $P2VP_{68}$-*b*-$PFMA_{41}$ micelles with different concentration formed after the seed solution in *i*-PrOH was annealed at 65 ^oC for 1 h followed by cooling to 23 ^oC. Representative TEM images are included in Figure S8.

C (mg / mL)	L_n (nm)	L_w (nm)	L_w/L_n	σ (nm)	σ/L_n
1.0	214	220	1.03	38	0.18
0.5	299	308	1.03	50	0.17
0.1	318	331	1.04	63	0.20
0.05	325	332	1.02	42	0.13

Table S4 Values of L_n, L_w, L_w/L_n, σ and σ/L_n of $P2VP_{68}$-*b*-$PFMA_{41}$ micelles formed after the seed solution in *i*-PrOH was annealed at 65 ^oC for different periods of time followed by cooling to 23 ^oC. Representative TEM images are included in Figure S9.

t (min)	L_n (nm)	L_w (nm)	L_w/L_n	σ (nm)	σ/L_n
5	193	203	1.05	43	0.22
10	251	269	1.07	66	0.26
20	287	299	1.04	57	0.20
30	309	318	1.03	54	0.17
60	320	333	1.04	64	0.19
120	314	327	1.04	63	0.20

Table S5 Values of L_n, L_w, L_w/L_n, σ and σ/L_n of $P2VP_{68}$-*b*-$PFMA_{41}$ micelles formed after the seed solution at 0.1 mg / mL in *i*-PrOH was annealed at 65 °C for 1 h followed by cooling to 23 °C and aging for different time. Representative TEM images are included in Figure S10.

t (h)	L_n (nm)	L_w (nm)	L_w/L_n	σ (nm)	σ/L_n
0	169	174	1.03	28	0.17
1	214	225	1.05	46	0.22
2	239	246	1.03	40	0.17
4	293	302	1.03	52	0.18
8	318	331	1.04	63	0.19
16	325	338	1.04	65	0.20

Table S6 Values of L_n, L_w, L_w/L_n, σ and σ/L_n of $P2VP_{68}$-*b*-$PFMA_{41}$ micelles prepared by annealing the pre-annealed cylindrical micelle seeds at 75 °C for 1 h, cooling to 23 °C. The original seeds were pre-annealed at 45 °C, 55 °C, and 65 °C for 1 h, cooled to 23 °C and aged for 24 h before the second annealing. Representative TEM images are included in Figure S11.

first annealing temperature (°C)	L_n (nm)	L_w (nm)	L_w/L_n	σ (nm)	σ/L_n
45	704	736	1.05	151	0.22
55	535	568	1.06	134	0.25
65	458	481	1.05	104	0.23

Table S7 Characteristics of $P2VP_{68}$-*b*-$PFMA_{41}$ micelles formed after the seed solution in *i*-PrOH was annealed at 70 °C for 1 h followed by cooling to 23 °C at 0.1 mg / mL or 0.2 mg / mL. The cylindrical micelles were characterized 16 h and 6 months after the thermal annealing, respectively. Representative TEM images are included in Figure S13.

	L_n [a] (nm)	L_w [a] (nm)	L_w/L_n [a]	σ [a] (nm)	σ/L_n [a]	% [b]	D_h [c] (nm)	PDI [c]
0.1 mg / mL, 16 h	462	471	1.02	65	0.14	0.8	N.A.	
0.1 mg / mL, 6 months	460	478	1.03	78	0.14	1		
0.2 mg / mL, 16 h	457	466	1.02	64	0.14	0.9	183	0.35
0.2 mg / mL, 6 months	458	469	1.02	71	0.15	13	204	0.41

a: obtained by measuring from TEM images, only the lengths of uncoupled cylindrical micelles were measured; b: the percentage population of end-coupled cylindrical micelles among all micelles, as counted from TEM images; c: obtained from DLS.

Table S8 Characteristics of $P2VP_{68}$-*b*-$PFMA_{41}$ micelles formed after the seed solution in *i*-PrOH was annealed (0.1 mg / mL, 2 mL) with 0.2 mg of F-dye at 80 °C for 1 h followed by cooling to 23 °C. Representative TEM images are included in Figure S16.

	L_n (nm)	L_w (nm)	L_w/L_n	σ (nm)	σ/L_n
loaded cylindrical micelle	2155	2236	1.02	313	0.15

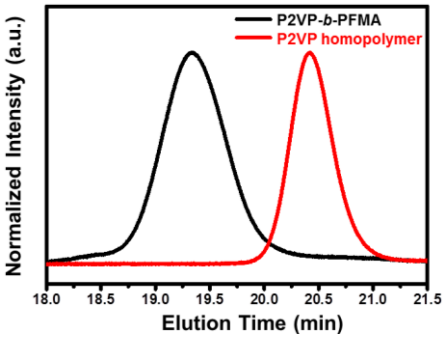

Figure S1 Normalized GPC refractive index (RI) traces of the P2VP homopolymer (red) and $P2VP_{68}$-*b*-$PFMA_{41}$ diblock copolymer (black). THF was used as the eluent and the concentration was ca.1 mg / mL.

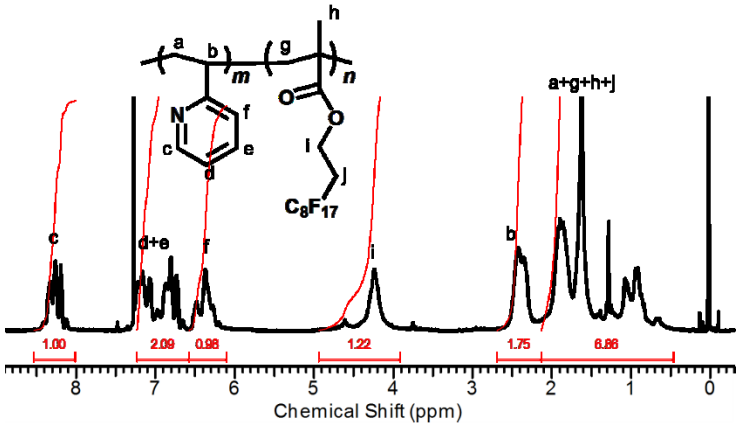

Figure S2 ^{1}H NMR spectrum of the $P2VP_{68}$-*b*-$PFMA_{41}$ diblock copolymer. $CDCl_3$ was used as the solvent.

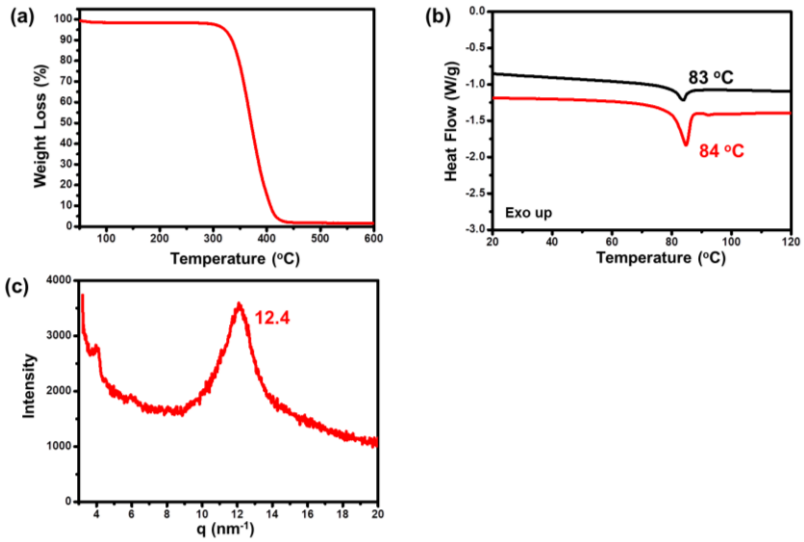

Figure S3 (a) TGA trace of the $P2VP_{68}$-*b*-$PFMA_{41}$ diblock copolymer; (b) DSC traces of the bulk $P2VP_{68}$-*b*-$PFMA_{41}$ diblock copolymer (red) and dried cylindrical micelles (black); (c) WAXS spectrum of the bulk sample of the diblock copolymer.

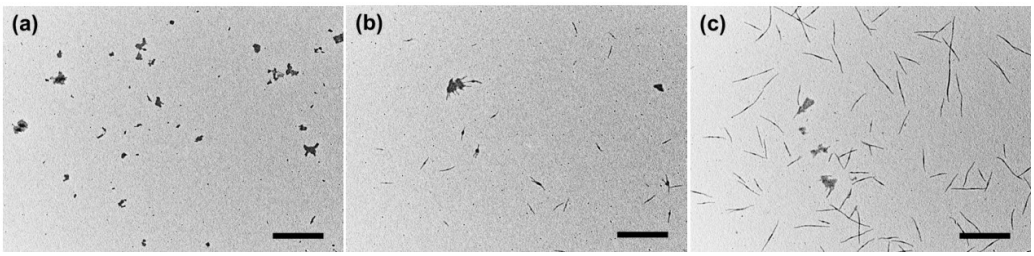

Figure S4 TEM images of the micelles formed by directly dispersing the $P2VP_{68}$-*b*-$PFMA_{41}$ diblock copolymer in *i*-PrOH at (a) 23 ^{o}C, (b) 60 ^{o}C, and (c) 70 ^{o}C for 1 h and then aged at 23 ^{o}C for overnight. Scale bars are 1 μm.

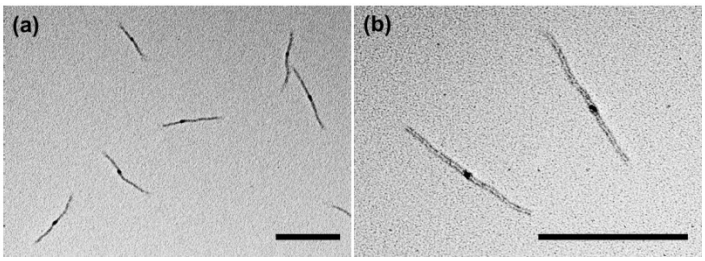

Figure S5 TEM images of the cylindrical micelles obtained by annealing the *i*-PrOH solution of seeds (0.1 mg / mL) at 70 ^{o}C: (a) no staining, (b) stained with RuO_4. Scale bars are 500 nm. The diameter of the cylindrical micelles is 17.2 ± 1.5 nm (without staining) or 18.1 ± 1.2 nm (with staining).

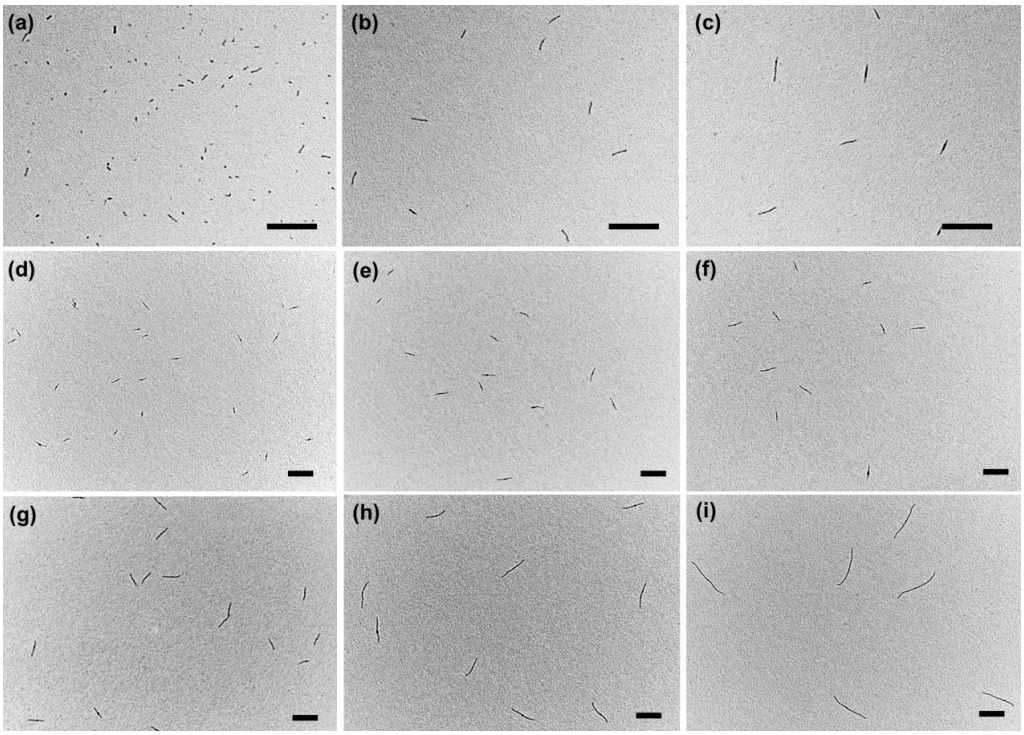

Figure S6 TEM images of the cylindrical micelles obtained by annealing the *i*-PrOH solution of seeds (0.1 mg / mL) at (a) 35 ^{o}C; (b) 40 ^{o}C; (c) 45 ^{o}C; (d) 50 ^{o}C; (e) 55 ^{o}C; (f) 60 ^{o}C; (g) 65 ^{o}C; (h) 70 ^{o}C; (i) 75 ^{o}C. The length information of all the samples is summarized in Table S2. Scale bars are 500 nm.

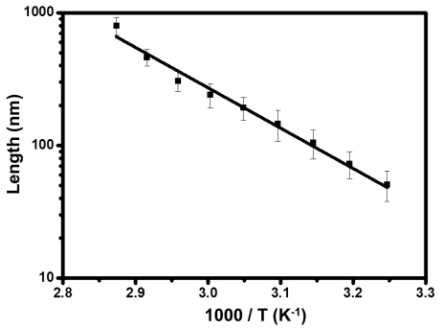

Figure S7 Semilogarithmic plots of micelle length L_n versus 1000/T [K^{-1}], where T is the dissolution temperature (from 35 ^oC to 75 ^oC). (error bars are the standard deviations σ for the length distribution). The straight line represents the best fit for the points of T to $\ln(L_n)$ = A-E/RT, where A is a constant.

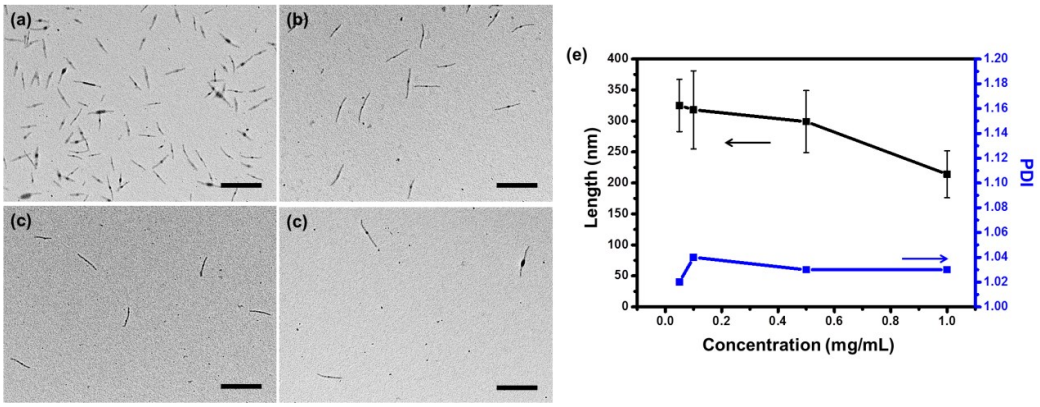

Figure S8 TEM images of the cylindrical micelles obtained by annealing the *i*-PrOH solutions of seeds with a concentration of (a) 1.0 mg / mL; (b) 0.5 mg / mL; (c) 0.1 mg / mL; (d) 0.05 mg / mL. Scale bars are 500 nm. (e) Number-average micelle length L_n and PDI vs concentration (error bars are the standard deviations σ in length). The solid line is a guide for eye guidance. The details of the length information of all the three samples are summarized in Table S3.

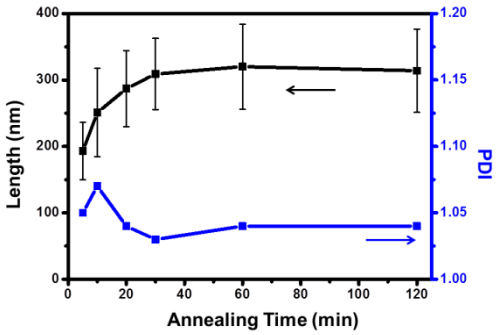

Figure S9 Annealing time dependence of L_n of the cylindrical micelles obtained by annealing the *i*-PrOH solutions of seeds at 65 ^oC for desired time period, followed by cooling to 23 ^oC. The error bars are the standard deviations σ in length for each sample. The solid line is a guide for eye guidance. The details of the length information of all the six samples are summarized in Table S4.

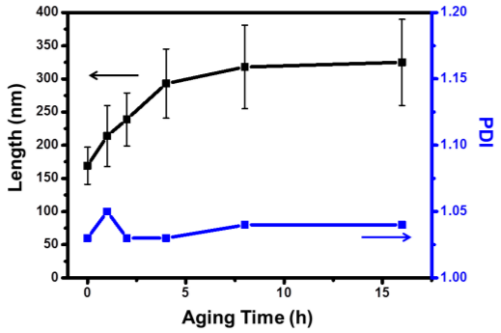

Figure S10 Aging time dependence of length L_n and PDI of the cylindrical micelles from P2VP$_{68}$-*b*-PFMA$_{41}$ obtained by annealing the *i*-PrOH solutions of seeds at 0.1 mg / mL in *i*-PrOH at 65 ^{o}C, followed by cooling to 23 ^{o}C. The error bars are the standard deviations σ in length for each sample. The solid line is a guide for eye guidance. The details of the length information of all the six samples are summarized in Table S5.

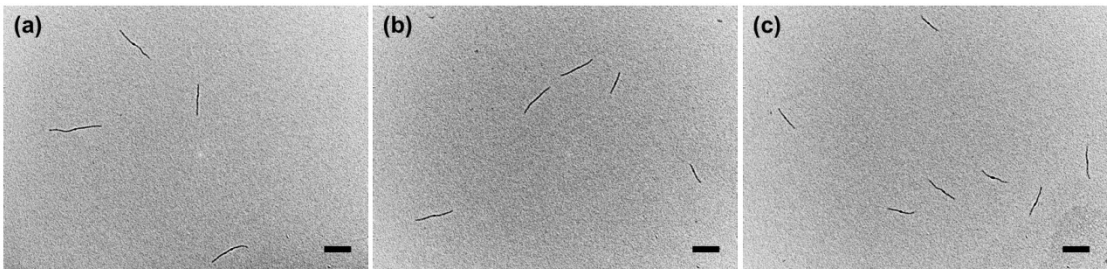

Figure S11 TEM images of cylindrical micelles (0.1 mg / mL) prepared by annealing the pre-annealed cylindrical micelle seeds at 75 ^{o}C for 1 h, cooling to 23 ^{o}C. The original seeds were pre-annealed at (a) 45 ^{o}C, (b) 55 ^{o}C, and (c) 65 ^{o}C for 1 h, cooled to 23 ^{o}C and aged for 24 h before the second annealing. Scale bars are 500 nm. The details of the length information of all the three samples are summarized in Table S6.

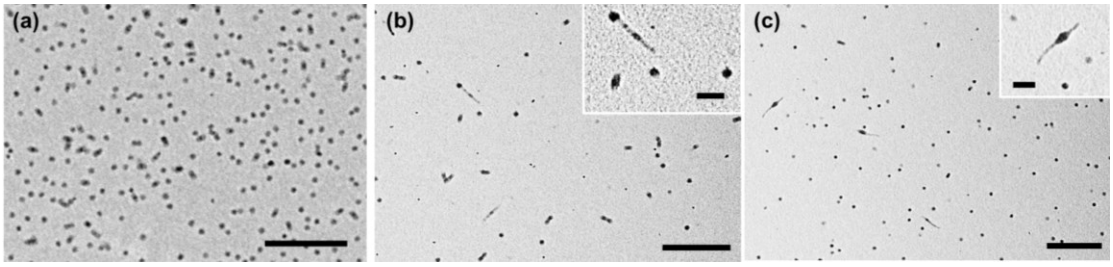

Figure S12 TEM images of the samples for seeded-growth attempts. Samples are prepared by adding 10 μL of chloroform solution (2.0 mg / mL) of P2VP$_{68}$-*b*-PFMA$_{41}$ into the *i*-PrOH solution of (a) seeds (1 mL, 0.01 mg / mL) and aged at 23 ^{o}C for 1 month; (b) cylindrical micelles (1 mL, 0.01 mg / mL) at 23 ^{o}C; and (c) cylindrical micelles (1 mL, 0.01 mg / mL) at 45 ^{o}C. The cylindrical micelles here were prepared by annealing the seeds solution (L_n = 42 nm, PDI = 1.07; 0.1 mg / mL) at 50 ^{o}C for 60 min, cooled to 23 ^{o}C, and aged at 23 ^{o}C for 24 h before use (L_n = 146 nm, PDI = 1.07). Scale bars are 500 nm in the images and 200 nm in the insets.

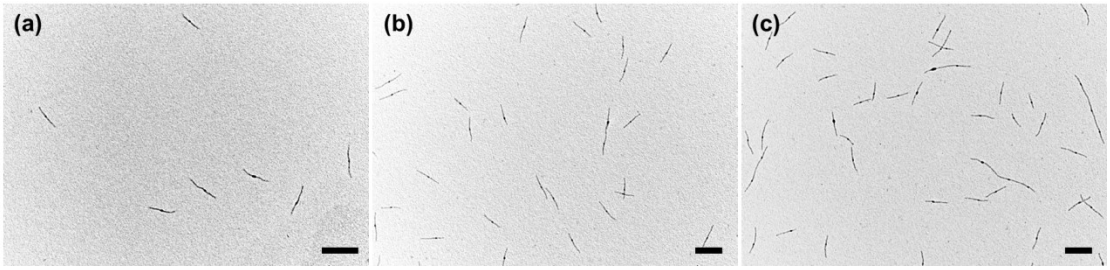

Figure S13 Additional TEM images of the cylindrical micelles at a concentration of (a) 0.1 mg / mL, and (b, c) 0.2 mg / mL . Cylindrical micelles prepared by (b) annealing the *i*-PrOH solutions of seeds at 70 ^{o}C for 1 h and cooling to 23 ^{o}C, and then (a, c) were aged at 23 ^{o}C for 6 months. The length information of all the samples is summarized in Table S7. Scale bar is 500 nm.

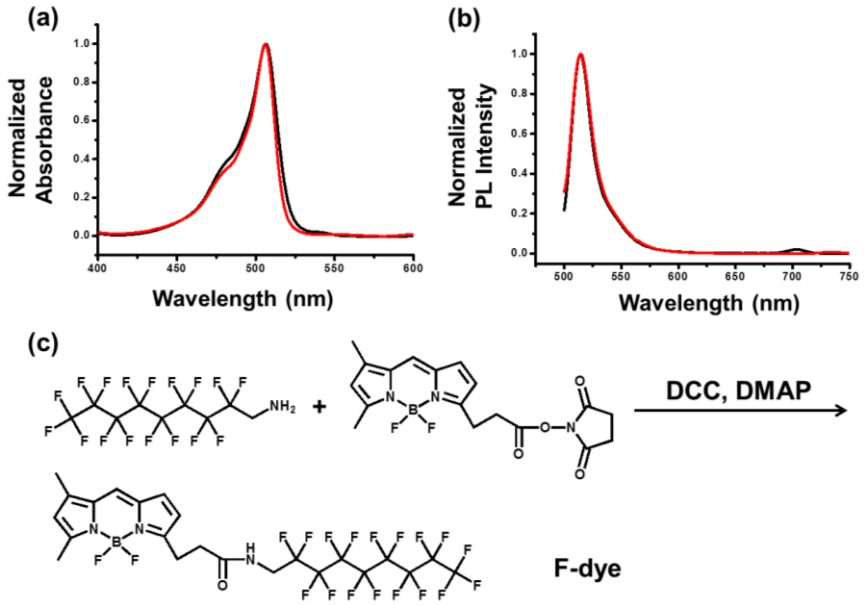

Figure S14 UV-vis absorbance spectrum (a), and fluorescence spectrum (b) (excitation wavelength = 480 nm) of the *i*-PrOH solution of F-dye (black) and F-dye-containing micelle (red). (c) The synthesis route used for the F-dye molecule.

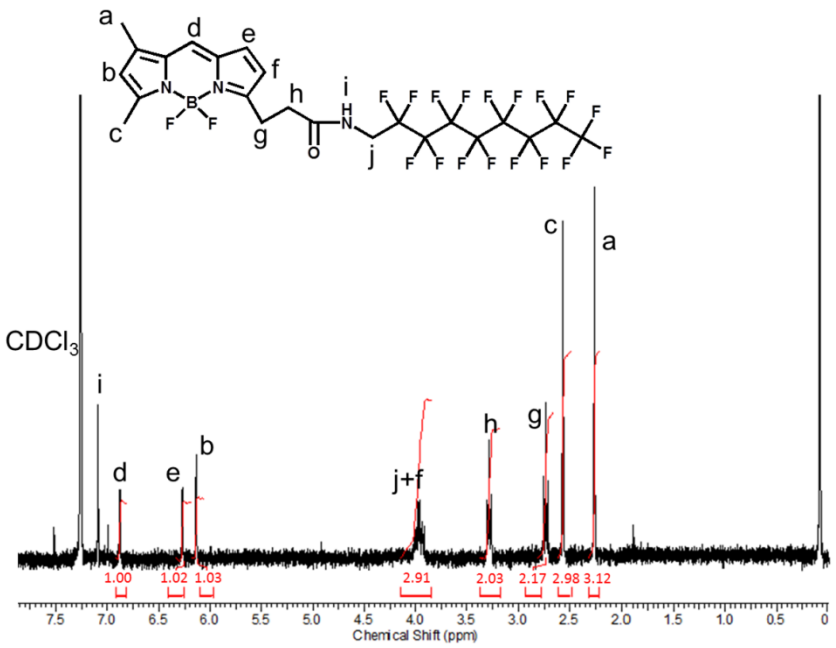

Figure S15 ^{1}H NMR spectrum of the F-dye molecule in $CDCl_3$.

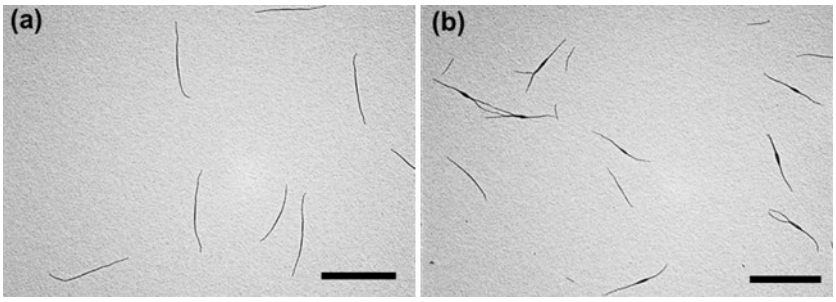

Figure S16 Additional TEM images of the F-dye-containing cylindrical micelles (0.1 mg / mL in *i*-PrOH) prepared via thermal annealing the *i*-PrOH solutions of seeds at 80 ^{o}C with F-dye loading ratios (F-dye : cylindrical micelles, mass %) of 3 % (a), 11 % (b). The length information for all the samples are summarized in Table S8. Scale bars are 2 μm.

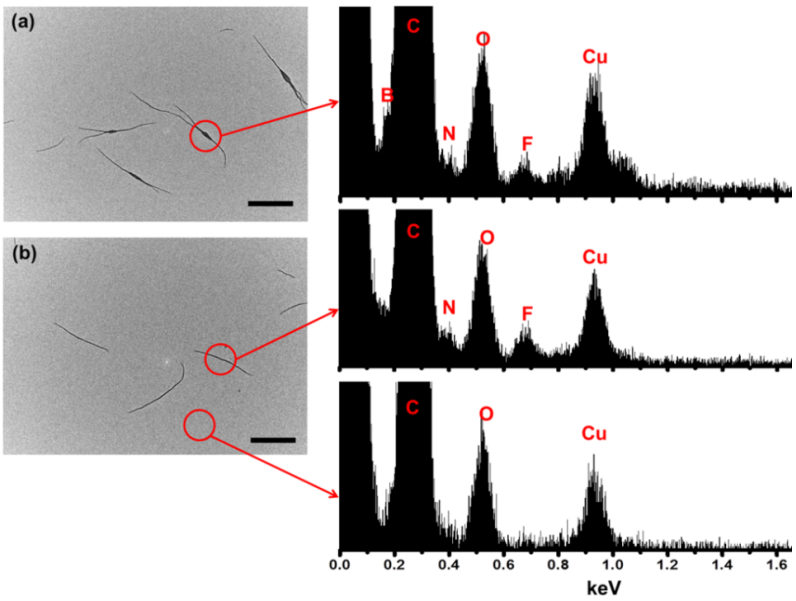

Figure S17 TEM images and EDX spot (the location of an EDX spot (spot diameter 25 nm) analysis indicated by the circle in the TEM images) analysis of the (a) F-dye-loaded cylindrical micelles (11 % of loading), and (b) cylindrical micelles without loading in *i*-PrOH. The EDX lines at ca. 0.9 keV are copper peaks due to the copper grid substrate. Scale bars are 500 nm.

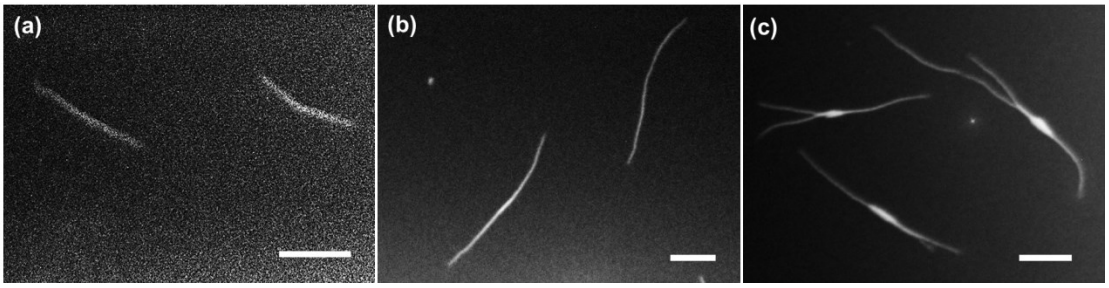

Figure S18 Dark field TEM images of the cylindrical micelles (a) without loading and obtained via annealing at 75 ^{o}C, (b) with 3 % by mass loading of F-dye, and (c) 11% by mass loading of F-dye (F-dye : cylindrical micelles, w.t.) in *i*-PrOH. Scale bars are 500 nm.

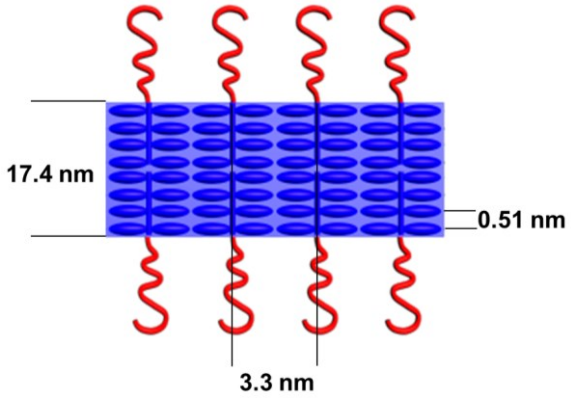

Scheme S1 Schematic illustration of the cross-sectional structure of the cylindrical micelles, based on the data obtained from X-ray scattering.

References:

(1) Gao, Y.; Li, X. Y.; Hong, L. Z.; Liu, G. J. *Macromolecules* **2012**, *45*, 1321-1330.

(2) Imae, T.; Tabuchi, H.; Funayama, K.; Sato, A.; Nakamura, T.; Amaya, N. *Colloids Surf., A* **2000**, *167*, 73–81.

(3) Pindak, R.; Moncton, D. E.; Davey, S. C.; Goodby, J. W. *Phys. Rev. Lett.* **1981**, *46*, 1135-1138.

(4) De Jeu, W. H.; De Poorter, J. A. *Phys. Lett. A* **1977**, *61*, 114-116.

(5) Gilroy, J. B.; Rupar, P. A.; Whittell, G. R.; Chabanne, L.; Terrill, N. J.; Winnik, M. A.; Manners, I.; Richardson, R. M. *J. Am. Chem. Soc.* **2011**, *133*, 17056-17062.

(6) Albertini, G.; Melone, S.; Poeti, G.; Rustichelli, F.; Torquati, G. *Mol. Cryst. Liq. Cryst.* **1984**, *104*, 121-130.

(7) de Jeu, W. H.; Ostrovskii, B. I.; Shalaginov, A. N. *Rev. Mod. Phys.* **2003**, *75*, 181-235.

(8) Hayward, D.W.; Whittell, G.R.; Gilroy, J.B.; Manners, I.; Richardson, R.M. *Liq. Cryst.*, **2016**, 43, 1148-1159.

(9) Qian, J. S.; Guerin, G.; Lu, Y. J.; Cambridge, G.; Manners, I.; Winnik, M. A. *Angew. Chem. Int. Ed.* **2011**, *50*, 1622-1625.

(10) Li, X.; Gao, Y.; Xing, X.; Liu, G. *Macromolecules* **2013**, *46*, 7436-7442.

(11) Mandelke.L; Allou, A. L.; Gopalan, M. *J. Phys. Chem.* **1968**, *72*, 309-318.

(12) Lammertink, R. G. H.; Hempenius, M. A.; Manners, I.; Vancso, G. J. *Macromolecules* **1998**, *31*, 795-800.

(13) Qian, J. S.; Li, X. Y.; Lunn, D. J.; Gwyther, J.; Hudson, Z. M.; Kynaston, E.; Rupar, P. A.; Winnik, M. A.; Manners, I. *J. Am. Chem. Soc.* **2014**, *136*, 4121-4124.

(14) Schmelz, J.; Schedl, A. E.; Steinlein, C.; Manners, I.; Schmalz, H. *J. Am. Chem. Soc.* **2012**, *134*, 14217-14225.

(15) Petzetakis, N.; Dove, A. P.; O'Reilly, R. K. *Chem. Sci.* **2011**, *2*, 955-960.

(16) He, W. N.; Zhou, B.; Xu, J. T.; Du, B. Y.; Fan, Z. Q. *Macromolecules* **2012**, *45*, 9768-9778.